Science Robotics
AAAS

# Supplementary Materials for

## Toward a living soft microrobot through optogenetic locomotion control of *Caenorhabditis elegans*

Xianke Dong *et al*.

Corresponding author: Xinyu Liu, xyliu@mie.utoronto.ca

Published 30 June 2021, *Sci. Robot.* ***6***, eabe3950 (2021)
DOI: 10.1126/scirobot.abe3950

**The PDF file includes:**

Figs. S1 to S10

**Other Supplementary Material for this manuscript includes the following:**

Movies S1 to S9

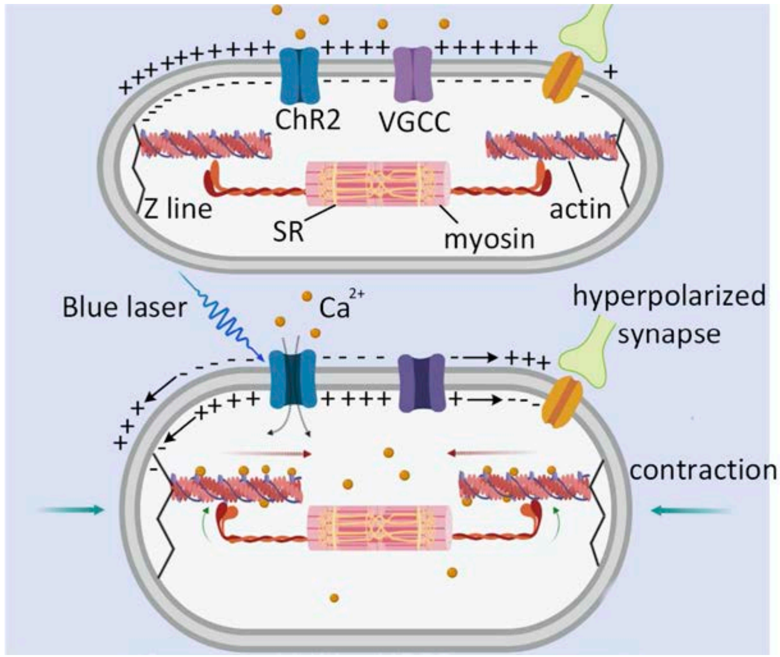


**Fig. S1. Molecular process of muscular optogenetics of *C. elegans*.** Naturally, the body wall muscle cells of a *C. elegans* are activated by the acetylcholine released from motor neurons. In our experiments, the ZM5398 worms were pre-treated with ivermectin, which primarily hyperpolarizes the worm neurons, and also slightly hyperpolarizes muscle cells (*39*). After the ivermectin treatment, the worms were paralyzed. This figure shows the biological pathway regulating the optical excitation of worm muscle cells. Upon illumination of micropatterned blue laser beams and in the presence of all-trans-retinal (ATR), the ChR2 ion channels on the muscle cell membrane open to allow the influx of $Ca^{2+}$ ions (*33*). The entry of $Ca^{2+}$ initiates membrane depolarization that propagates along the sarcolemma and activates the voltage-gated calcium channels (*33*), which finally triggers the release of $Ca^{2+}$ stored in sarcoplasmic reticulum into the cytosol. These $Ca^{2+}$ ions bind to troponin, change its shape, and lead to the displacement of actin and myosin with the energy supplied by ATP (*33*). In general, the illuminated body muscle cells of the ZM5398 worms contract and shrink their lengths, and the muscle cell contractions cause bending of the illuminated worm body part. Created with Biorender.com.

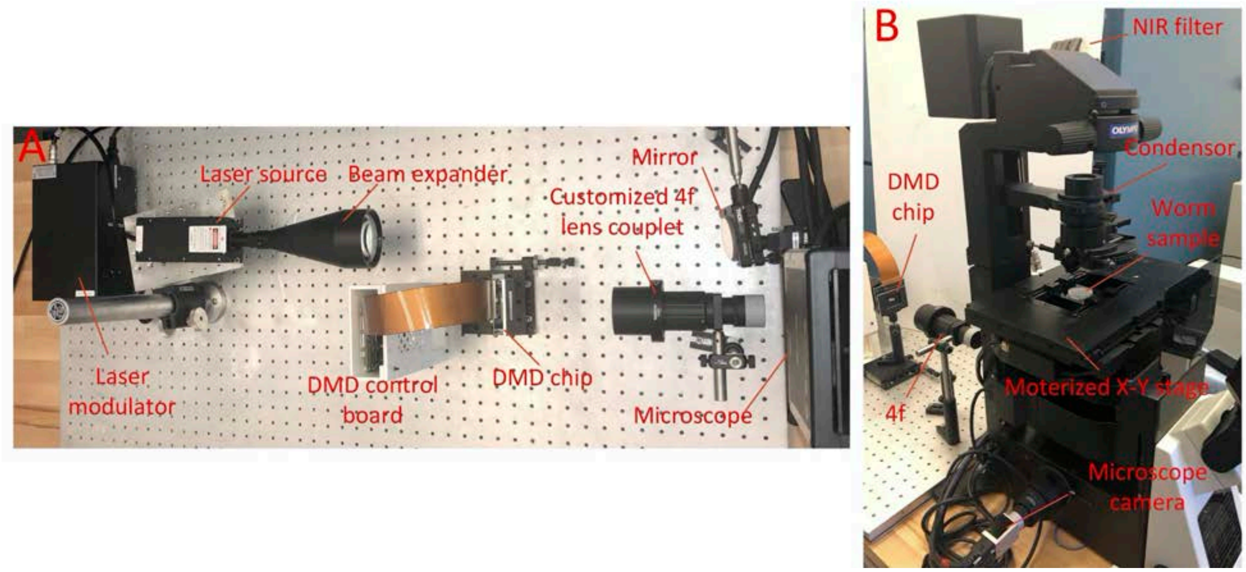


**Fig. S2. Photography of the pattern-light projection system constructed on inverted microscope.**

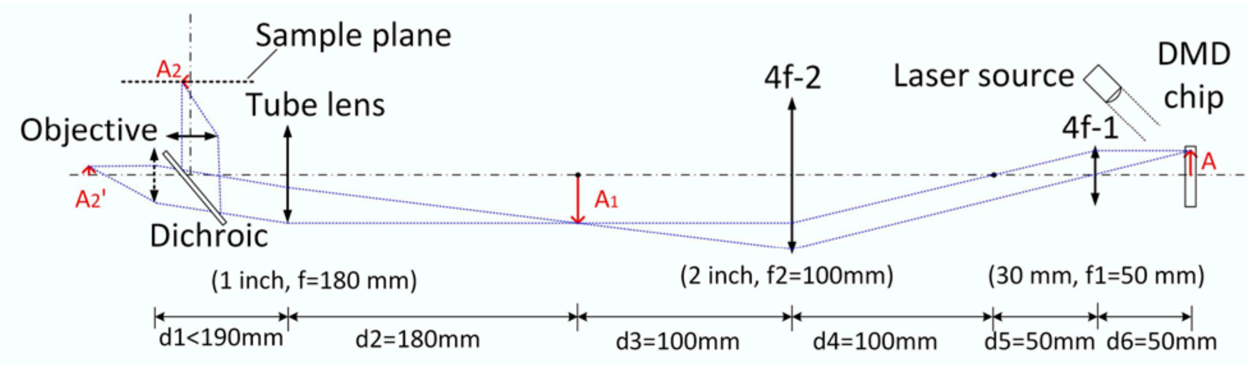


**Fig. S3. Optics configuration of the projection system.**

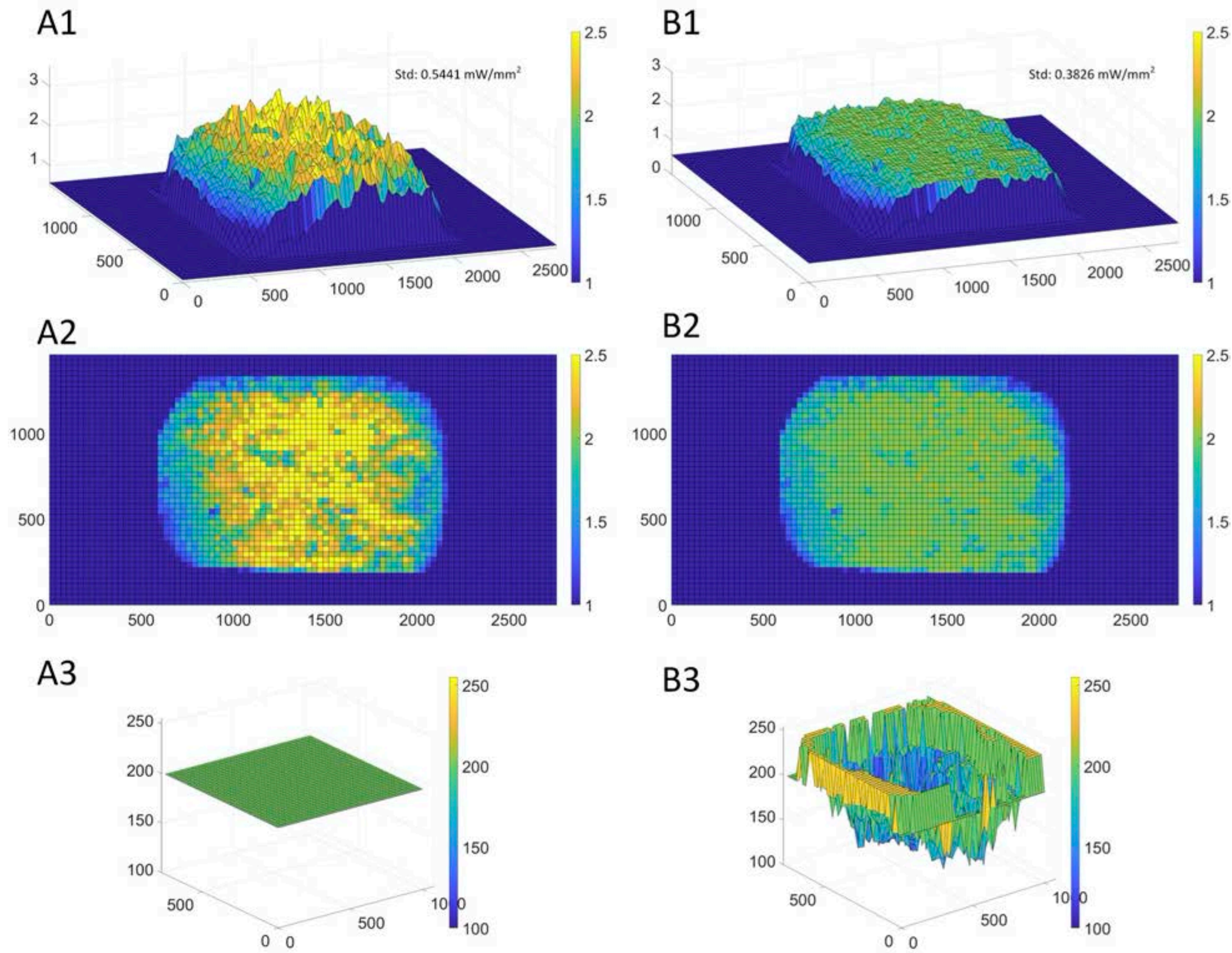


**Fig. S4. The laser intensity compensation results by automatic adjusting the duty ratio of the DMD pixels**. **(A1-A2)** The intensity distribution before compensation. **(A3)** The corresponding pixel intensities (8-bit depth) on the DMD chip. **(B1-B2)** The intensity distribution after automatic adjustment of pixel duty ratio. **(B3)** The pixel intensities after adjustment.

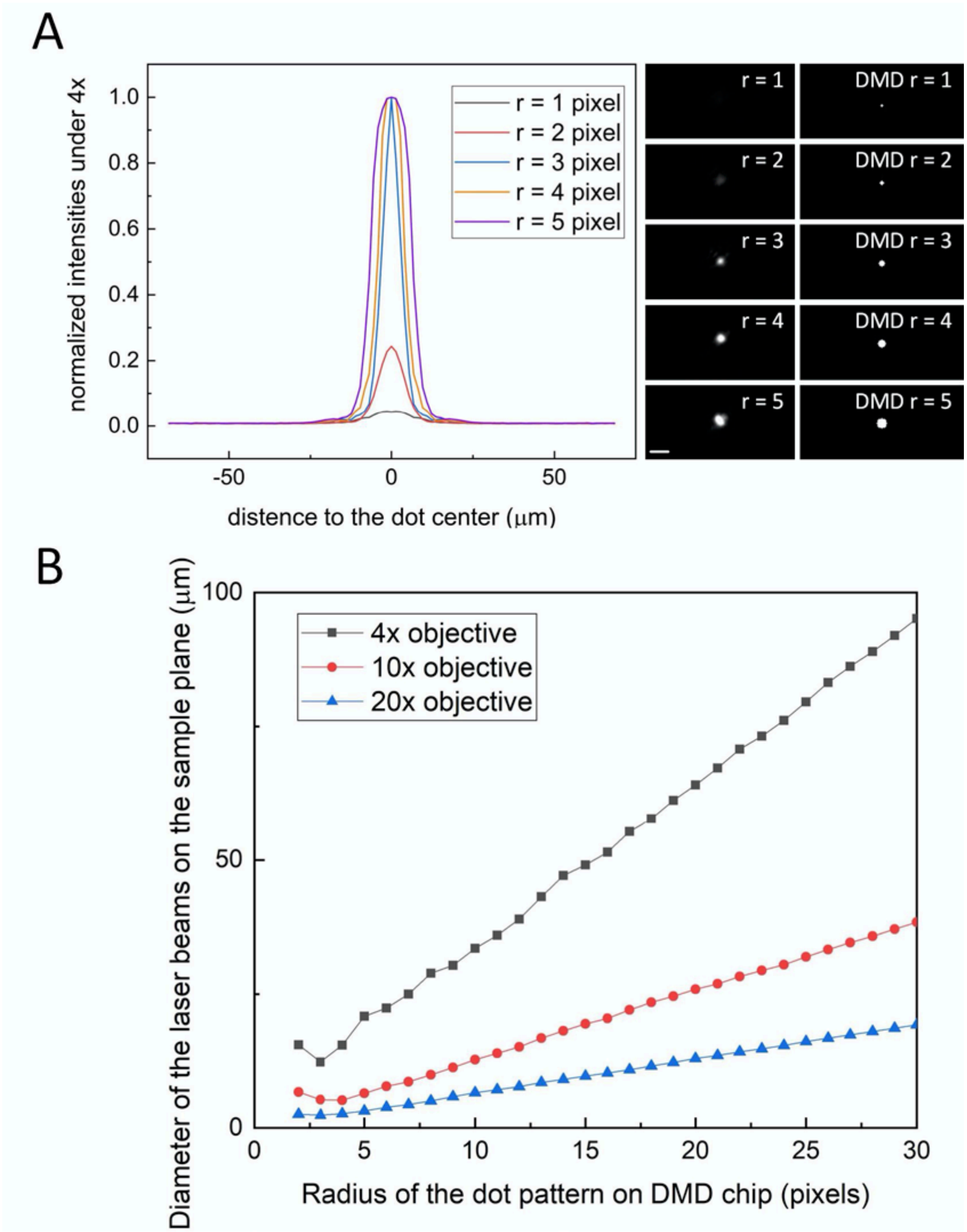


**Fig. S5. Resolution measurements of the patterned-light illumination system. (A)** The measured intensities of dot laser pattern with the size from 1 to 5 DMD pixels in microscope camera. **(B)** The measured beam size on the microscope sample plane with respect to various pattern size on DMD chip.

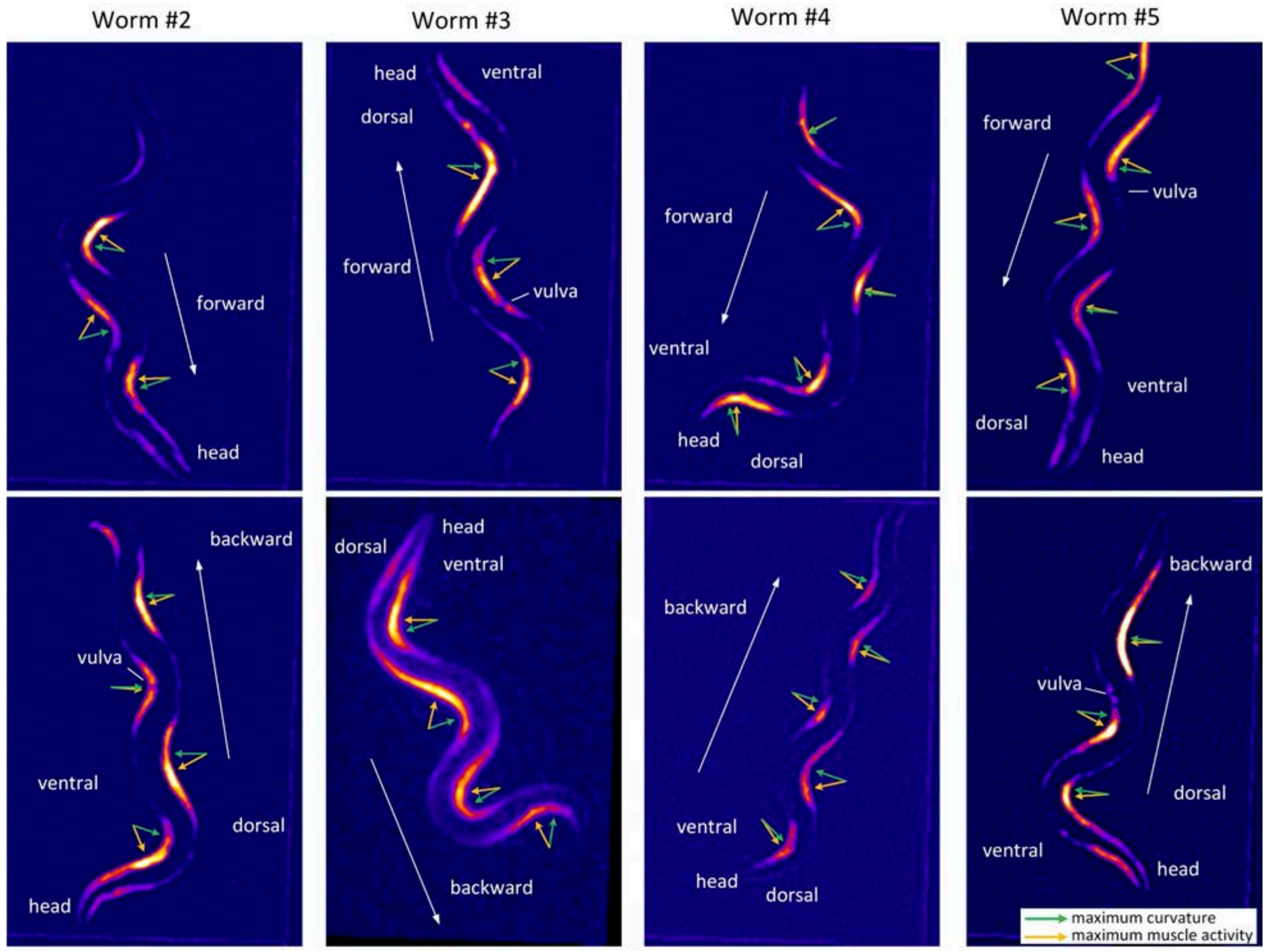


**Fig. S6. The fluorescent images for the worm muscular activity during natural crawling on agar.** Strain AQ2953 *ljIs 131* [*Pmyo-3-GCaMP3::RFP*] was used. *GCaMP3* signal was recorded and normalized with the *RFP* signal in dual-view camera. In the image, bright body sections indicate high muscular activity.

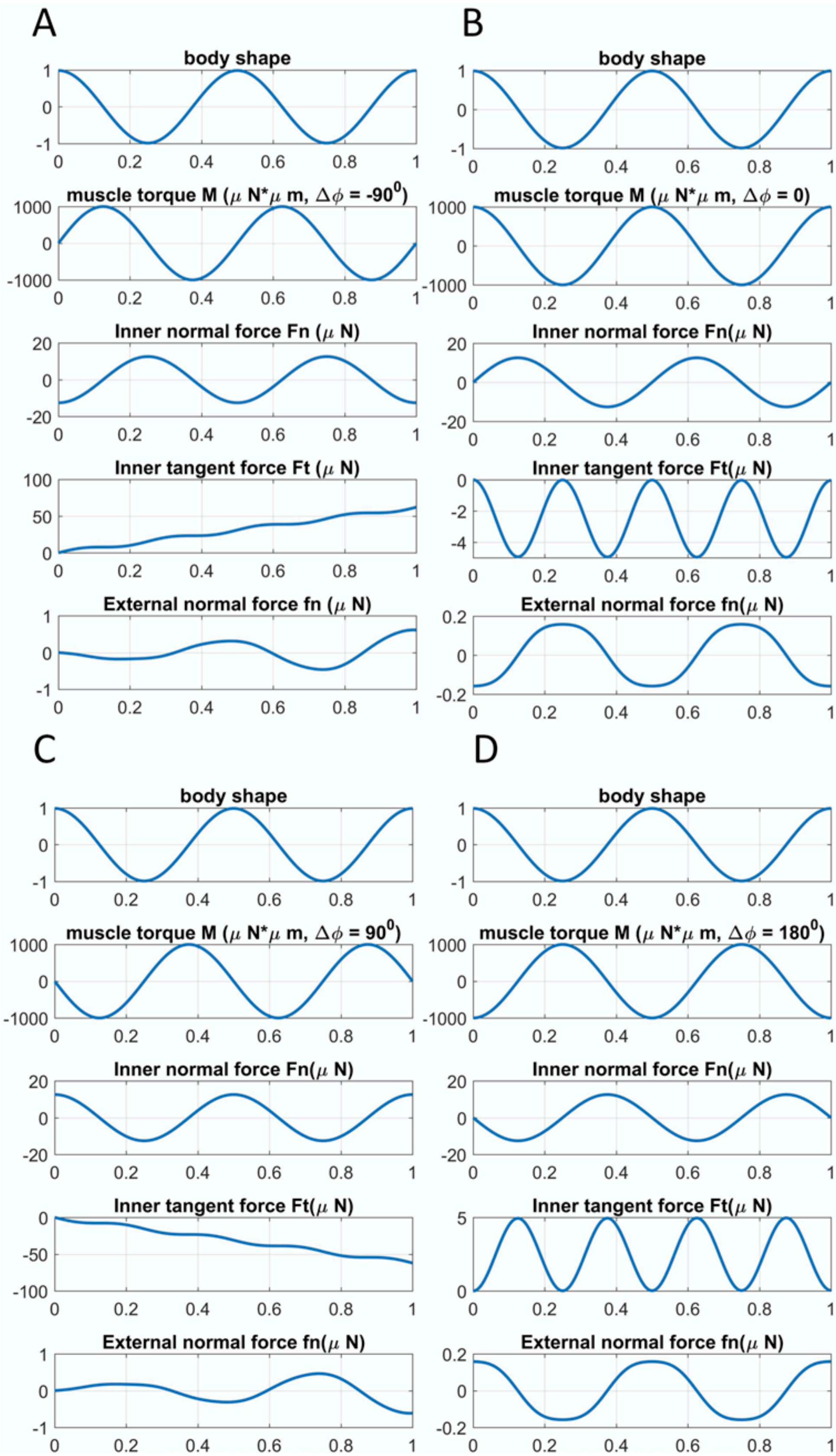


**Fig. S7. The simulation results for the phase difference of (A)** $\Delta\varphi = -\pi/2$, **(B)** $\Delta\varphi = 0$, **(C)** $\Delta\varphi = \pi/2$, **(D)** $\Delta\varphi = \pi$, **respectively.**

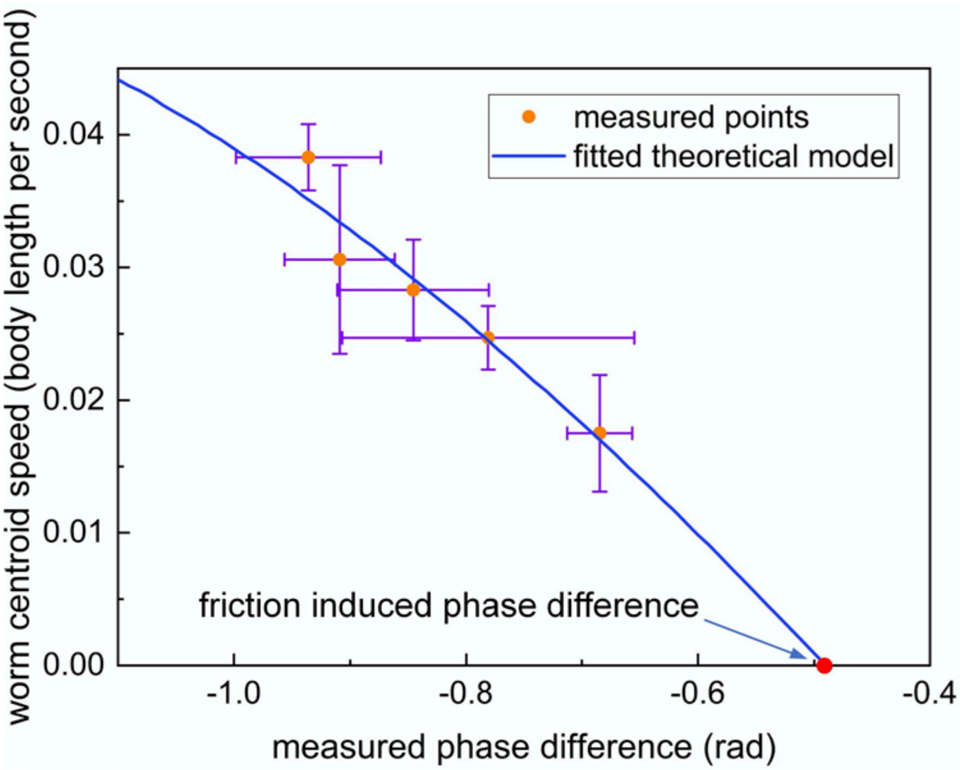


**Fig. S8. The change of worm speed with respect to measured phase difference (n=5).** In the experiment, the measured worm moving speed reduced monotonically as the calculated phase difference $\Delta\varphi$ amplitude decreased within $\left(-\frac{\pi}{2}, 0\right)$, which supports the proposed thrust force theory.

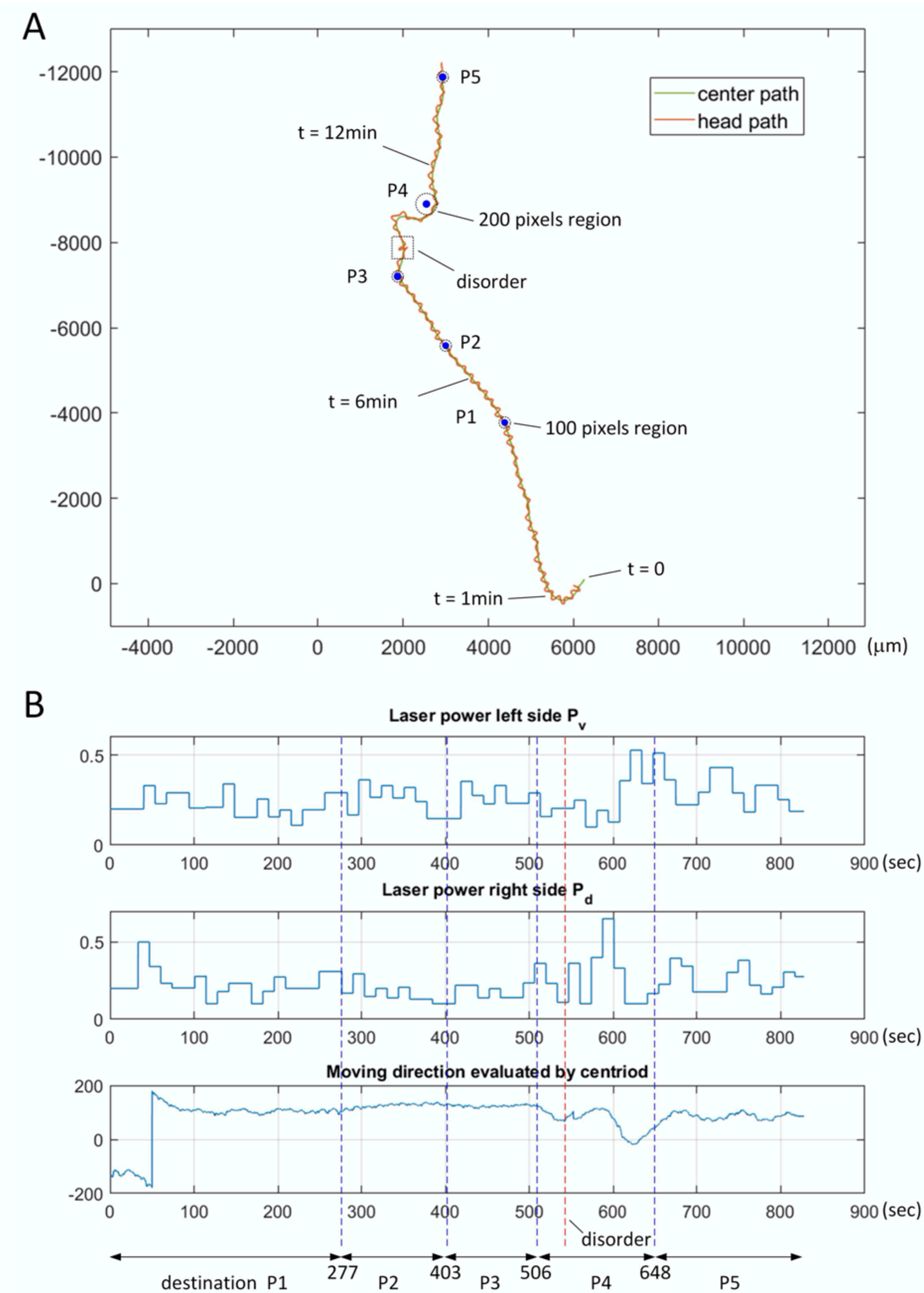


**Fig. S9. The data for the experiment of controlling the worm pass through a maze. (A)** The worm movement path on the agar. **(B)** The laser intensity input and the measured moving direction. The moving direction of the RoboWorm was measured from -180 degrees to 180 degrees.

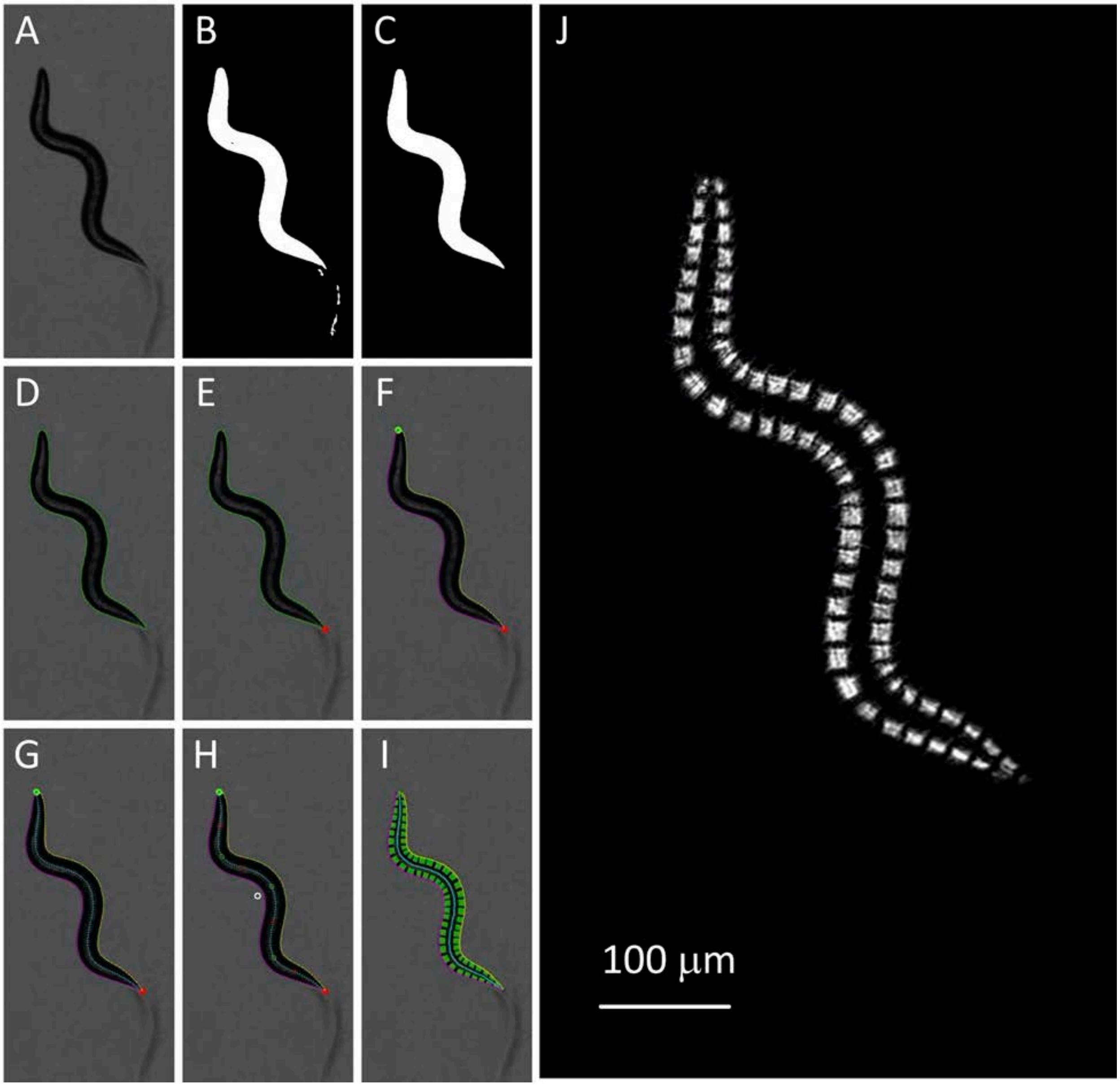


**Fig. S10. The image processing algorithms for the real-time tracking of *C. elegans*. (A)** The original image grabbed by the microscope camera. **(B)** The binarized image. **(C)** The purified binarized image. **(D)** The contour of the worm. **(E)** The tail detection on the worm image. **(F)** The head detection on the image. **(G)** The centerline calculation on the image. **(H)** The mass center and the curvature calculation. **(I)** The segmentation of the worm body. **(J)** The projected worm pattern on the microscope sample plane with 4× objective.